Spatiotemporally separated antigen uptake by alveolar dendritic cells and airway presentation to T cells in the lung

Emily E. Thornton,[1] Mark R. Looney,[2,4] Oishee Bose,[1] Debasish Sen,[1] Dean Sheppard,[3,4] Richard Locksley,[5] Xiaozhu Huang,[3,4] and Matthew F. Krummel[1]

[1]Department of Pathology, [2]Department of Laboratory Medicine, [3]Lung Biology Center, [4]Department of Medicine, and [5]Howard Hughes Medical Institute, University of California, San Francisco, San Francisco, CA 94143

Asthma pathogenesis is focused around conducting airways. The reasons for this focus have been unclear because it has not been possible to track the sites and timing of antigen uptake or subsequent antigen presentation to effector T cells. In this study, we use two-photon microscopy of the lung parenchyma and note accumulation of CD11b$^+$ dendritic cells (DCs) around the airway after allergen challenge but very limited access of these airway-adjacent DCs to the contents of the airspace. In contrast, we observed prevalent transepithelial uptake of particulate antigens by alveolar DCs. These distinct sites are temporally linked, as early antigen uptake in alveoli gives rise to DC and antigen retention in the airway-adjacent region. Antigen-specific T cells also accumulate in the airway-adjacent region after allergen challenge and are activated by the accumulated DCs. Thus, we propose that later airway hyperreactivity results from selective retention of allergen-presenting DCs and antigen-specific T cells in airway-adjacent interaction zones, not from variation in the abilities of individual DCs to survey the lung.

CORRESPONDENCE
Matthew F. Krummel:
matthew.krummel@ucsf.edu

Abbreviations used: AM, alveolar macrophage; BAL, bronchoalveolar lavage; i.n., intranasal(ly); TLR, Toll-like receptor.

The tissue of the lung is a complex filigree, supporting gas exchange and presenting a large surface for antigen surveillance and uptake. This interface provides a classical example of the challenges of mucosal immunity; responses to environmental antigens need to be minimized, whereas the exposure to pathogens requires rapid local responses. The dominant symptoms of asthma, airway constriction and mucus accumulation, are the results of immune responses near airways. A rich body of literature has identified lung DCs and alveolar macrophages (AMs) as predominant phagocytic populations, both in the steady-state and in disease (Robinson et al., 1992; McWilliam et al., 1996; Belz et al., 2004; Holt, 2005; van Rijt et al., 2005; von Garnier et al., 2005; Sung et al., 2006; Grayson et al., 2007; Hammad et al., 2010). Although it is clear by depletion protocols that lung DCs play a major role in airway pathogenesis (Lambrecht et al., 1998; van Rijt et al., 2005), the spatial dynamics that define how and where they sample material and when and where they present antigen has not been assessed.

DCs in the lung, in contrast to AMs, are very effective at generating T cell responses (Belz et al., 2004) and are also instrumental in initiating and perpetuating T cell hyperresponsiveness associated with asthma (van Rijt et al., 2005; Hammad et al., 2010). CD103$^+$ and CD11b$^+$ subsets have been proposed to activate CD8 and CD4 responses, respectively (Jakubzick et al., 2008b). CD103$^+$ DCs have been shown to play important roles in viral responses (Ballesteros-Tato et al., 2010) and apoptotic cell uptake (Desch et al., 2011), but the localization and uptake capacity of these cells has not been addressed in the lung. Increased numbers of DCs are found in bronchoalveolar lavage (BAL) fluid of asthmatic patients after allergen challenge (Robinson et al., 1992; van Rijt et al., 2002), suggesting that their increase is associated with disease. In mice, upon OVA challenge in an OVA/alum mouse model of

The Rockefeller University Press $30.00
J. Exp. Med. Vol. 209 No. 6 1183-1199
www.jem.org/cgi/doi/10.1084/jem.20112667

The Journal of Experimental Medicine

asthma, lung tissue–associated DCs also increase in number and increase expression of co-stimulatory molecules (van Rijt et al., 2005). After depletion of DCs and macrophages with the CD11c-driven diphtheria toxin receptor, OVA-treated mice lose the hallmarks of asthma (van Rijt et al., 2005). Despite the large amount of data indicating the importance of DCs in allergic responses in the lung, their functions within the tissue have remained unclear.

Despite the wealth of studies on the trafficking of DCs from the lung taken from endpoint analyses, less is understood about the initial competition for antigens with the more populous AMs, specifically, how in situ movement and surveillance by DCs and AMs influences the fate of inhaled materials. The specific handling of antigens by DCs in the entire lung has largely been inferred from tracheal preparations. These have revealed DCs that project dendrites into but not through the tight junctions of epithelial cells (Jahnsen et al., 2006). A similar study highlighted tracheal DCs as interlinked sheets lining the mucosal surface (Lambrecht et al., 1998). The uptake of fluorescent particulate antigens and macromolecules that are too large to cross the epithelial border by lung DCs suggested that these cells have mechanisms to reach across into the airspace (Byersdorfer and Chaplin, 2001; Vermaelen et al., 2001). A prominent proposal is that breakdown in the epithelium, perhaps in response to Toll-like receptor (TLR) ligands, underlies pathogenesis (Lambrecht and Hammad, 2009). Increased DC motility has been observed in tracheal sections in response to epithelial recognition of TLR4 ligands (Hammad et al., 2009), and occasional dendritic extensions in tracheal DC preparations have been reported, although it is not clear that these are present under normal conditions (Hammad and Lambrecht, 2008). These extensions mimic similar dendrites that protrude (Rescigno et al., 2001), increasingly after injury or TLR signaling, into the lumen of the gut (Chieppa et al., 2006). In vitro studies using lung airway epithelium cultures have suggested that, though their cell bodies are often beneath the epithelium, DCs may protrude through epithelial tight junctions (Vermaelen et al., 2001; Blank et al., 2007), although the relevance of this to the whole lung remains undescribed.

It is well established that the majority of particulate antigen transport to the draining LNs is performed by DCs and not by passive carriage of antigen via the flow of afferent lymph. Diphtheria toxin–mediated depletion of lung DCs reduces antigen traffic to the LN (Vermaelen et al., 2001), and DC homing depends on CC-chemokine receptor 7 (Jakubzick et al., 2006; Hammad and Lambrecht, 2007; Wikstrom and Stumbles, 2007). Particle-bearing DCs that traffic to the LN can subsequently elicit T cell responses to proteins borne on the particulate (Byersdorfer and Chaplin, 2001). The late (adaptive) phase of asthma exacerbations begins only 8 h after antigen inhalation, which would provide little time for antigen traffic to the LN and T cell traffic back to the lung (Wenzel et al., 2007). How and where these allergens are presented to T cells to generate airway-localized inflammatory responses are not clear.

Two-photon imaging has previously been used to track the dynamic behavior of lymphocytes in LNs (Miller et al., 2002) and provides the possibility to assess cells deep within their native and complex tissues (Germain et al., 2006; Cahalan and Parker, 2008). For LNs, both intravital as well as organ explant models have been described, and the comparisons of these two has provided insight into when each is applicable. The use of two-photon microscopy for lung has previously been demonstrated with viable lung slices for the study of smooth muscle functions (Bergner and Sanderson, 2002), but the behavior of the immune system during allergy in these preparations has not been formally assessed. Recently, stabilized and ventilated intravital lung imaging has also become possible. Using this method, airflow and blood flow remain intact, and alveolar imaging is possible (Kreisel et al., 2010; Looney et al., 2011). Under such a preparation, tissue remains demonstrably viable and without evidence of immune infiltrate induced by the preparation (Looney et al., 2011).

In this study, we have applied two-photon live imaging of viable lung slices and intravital stabilized lung to discover the antigen surveillance and presentation dynamics in lung. We tested the hypothesis that surveillance changes at the cellular level after allergen challenge. Using CD11c-EYFP mice (Lindquist et al., 2004), which, by two-photon imaging, mark DCs and mark AMs only after allergen challenge, we were able to differentially track the behavior, antigen uptake, and cell–cell interactions of $CD11b^+$ DCs in viable lung tissue. We compared these activities on a per-cell basis, both in the steady-state and in the widely studied OVA model of allergic lung disease. Although other mucosa has demonstrated evidence of changes in motile behavior of DCs during insult, neither acute allergy induction nor treatment with bacterial LPS significantly changed their surveillance behaviors within the lung tissue. We also found that alveoli are unexpectedly the sites of the most robust DC air surveillance in the steady-state with highly dynamic dendrites that project across epithelial barriers. We captured examples of DCs ingesting particles directly from an alveolar atrium and found that DCs are extremely effective at phagocytosis of particulate antigens from this location. Airway DCs, which exhibit greater center of mass motility than parenchymal DCs, rarely send processes across the airway epithelium. We have been unable to detect either breakdown of the epithelium leading to DC access or increased extension after allergen challenge. However, antigen-bearing DCs accumulate near airways after allergen challenge. Concurrently, activated T cells accumulate in the same regions. Thus, accumulation of antigen-bearing DCs near airways, rather than changes in alveolar APC phagocytic function during surveillance, generates a local presentation mechanism. This represents the dominant variation in antigen handling and a likely driver of pathogenesis in allergic airways disease and asthma.

RESULTS

$CD11b^+$ DCs accumulate near allergic airways

To understand the nature of antigen processing for presentation to T cells as it occurs on and in the lung mucosa during

asthma, it was necessary to firmly establish the details of AM and DC populations as well as a system for marking these cells for imaging. We opted to perform all of these experiments in the context of the highly studied OVA challenge model of allergic lung disease, representing a subset of the features of some forms of human asthma (Blyth et al., 1996). The system is primarily based on a standard immunization strategy with OVA in alum (Fig. 1 A) followed by inhalation of OVA in the recall phase, which routinely results in robust responses including eosinophil infiltration (not depicted), airway hyperresponsiveness (Voehringer et al., 2006), and goblet cell hyperplasia (Blyth et al., 1996). In contrast, PBS inhalation does not result in significant changes in the lung.

To track AM and DC populations in real time, we took advantage of transgenic mice in which EYFP expression is driven under the control of the CD11c locus (CD11c-EYFP; Lindquist et al., 2004). FACS analysis showed that $CD11b^+$ DC numbers increased in the lungs of allergic mice (Fig. 1, B and C; gating strategy in Fig. S1, A and B) but showed also that CD11c-EYFP was expressed on all DC populations and AMs after allergen challenge (Fig. S1 C). Whereas $CD11b^+$ DCs, $CD103^+$ DCs, and AMs expressed similar levels of class II before allergen challenge, both DC populations upregulated class II expression after allergen challenge (not depicted). This is consistent with the ability to prime or reactivate T cells within the lung. With understanding of the CD11c-EYFP marker expression profile and this in situ maturation, we turned toward imaging to segregate DCs spatially and to use image analysis to deconvolve these populations.

We developed a technique for live cell imaging in the lung adapted from the previous work of Bergner and Sanderson (2002). In brief, lungs were filled with agarose, removed from the mouse, and sectioned into 300-µm sections using a vibratome (Fig. S2 A). Lung sections are maintained at 36°C in oxygenated media for imaging. Under these conditions, propidium iodide staining 4 h after imaging showed only modest cell death, confined to the cut face and distant from the sites of our imaging, which always began at least 50 µm beneath the cut site and proceeded downward (Fig. S2 B). Cell-autonomous behaviors and viability were evident from ciliary beating in the large airways (Video 1), which has been documented to be maintained under these conditions for 10 d (Bergner and Sanderson, 2002).

Tiling of large three-dimensional volumes obtained in this way confirms and highlights the dramatic expansion of $CD11c\text{-}EYFP^{hi}$ cells that we observed using flow cytometry and allowed us to spatially assign this to regions of the alveolar spaces and airways (Fig. 1 D). Quantification of cells showed accumulation of $EYFP^+$ cells near the airway after OVA challenge (Fig. 1 E). However, as would be predicted from the $CD11c^{hi}$ gate in the flow analysis, DCs were the dominant cells imaged under control conditions, whereas both DCs and AMs were visualized with this marker in the allergen challenge condition (Fig. S1). To resolve this, we took advantage of the distinct morphologies of these two cell types to separate them using automated image analysis. The AMs were distinguishable because of their very round shape, which is associated with a sphericity measure of >0.75, shown as the second peak of sphericity in the histogram representing the CD11c-EYFP population (Fig. 1 F). Side by side analysis of Siglec-F, a marker closely linked to AMs but not DCs, confirmed that this sphericity corresponded well to AM/DC distinction (Fig. 1 G). This morphological criterion in turn allowed us to separate these two cell types within images (Fig. 1 H) and ultimately to confirm that the majority of the DC accumulation observed by FACS was accounted for in the airway-adjacent DC populations with much less variation in the alveolar populations (Fig. 1 I).

Because the lung contains subpopulations of DCs, we also wanted to determine which subpopulations we were examining in our imaging system. By staining live lung sections from CD11c-EYFP mice with CD11b APC antibody, we were able to visualize the $CD11b^+$ and $CD11b^-$ DC populations (Fig. 1 J). Quantification of the resulting images shows that the DCs that accumulated near the airway were $CD11b^+$; however, $CD11b^+$ and $CD11b^-$ DCs were not otherwise strictly segregated by location within the lung (Fig. 1 K). In sum, this analysis indicated that inflammation during allergen challenge was largely associated with increased numbers of $CD11b^+$ DCs retained in the airway-adjacent region, where the pathology of asthma is most evident.

DCs in lung subregions behave differently

Although this imaging system provided much needed clarity about phagocyte accumulation after allergen challenge, the method also provided a route to directly analyze the behaviors of those cells in situ. By acquiring time-lapse videos of these viable lung slices, we were able to track these potential APCs. Using both the EYFP marking and the sphericity measures of Fig. 1, we found that DCs exhibited significant center of mass motility near airways, moving nondirectionally just below the surface of the epithelium. In contrast (with the exception of the rare CD11c-EYFP cell that moved within the lung parenchyma and was perhaps targeted toward lymphatics), there was generally very little motility in alveolar regions (Fig. 2 A and Video 2).

Quantification of the motility of many cells (as defined by the movement of the weighted center of their cell bodies) revealed speeds of ~2.5 µm/min near the airway surface, which was not appreciably altered under allergen challenge. In contrast to the more motile airway-adjacent DCs, DCs located near the alveoli were typically more stationary (mean velocity of 1–1.5 µm/min) under both conditions, possibly indicating different functions for DCs at the two locations. AMs, in contrast, only moved at very slow speeds after allergen challenge (<1 µm/min; Fig. 2 B). This slow motility of AMs was also similar in control animals, as assessed using the *c-fms*–EGFP mouse (Video 3); however, this data does not preclude the possibility of different behavior in the case of infection. Speed analysis is sometimes confounded by the possible jitter of cells accounting for an apparent center of mass movement, and so we performed analysis of the tracks

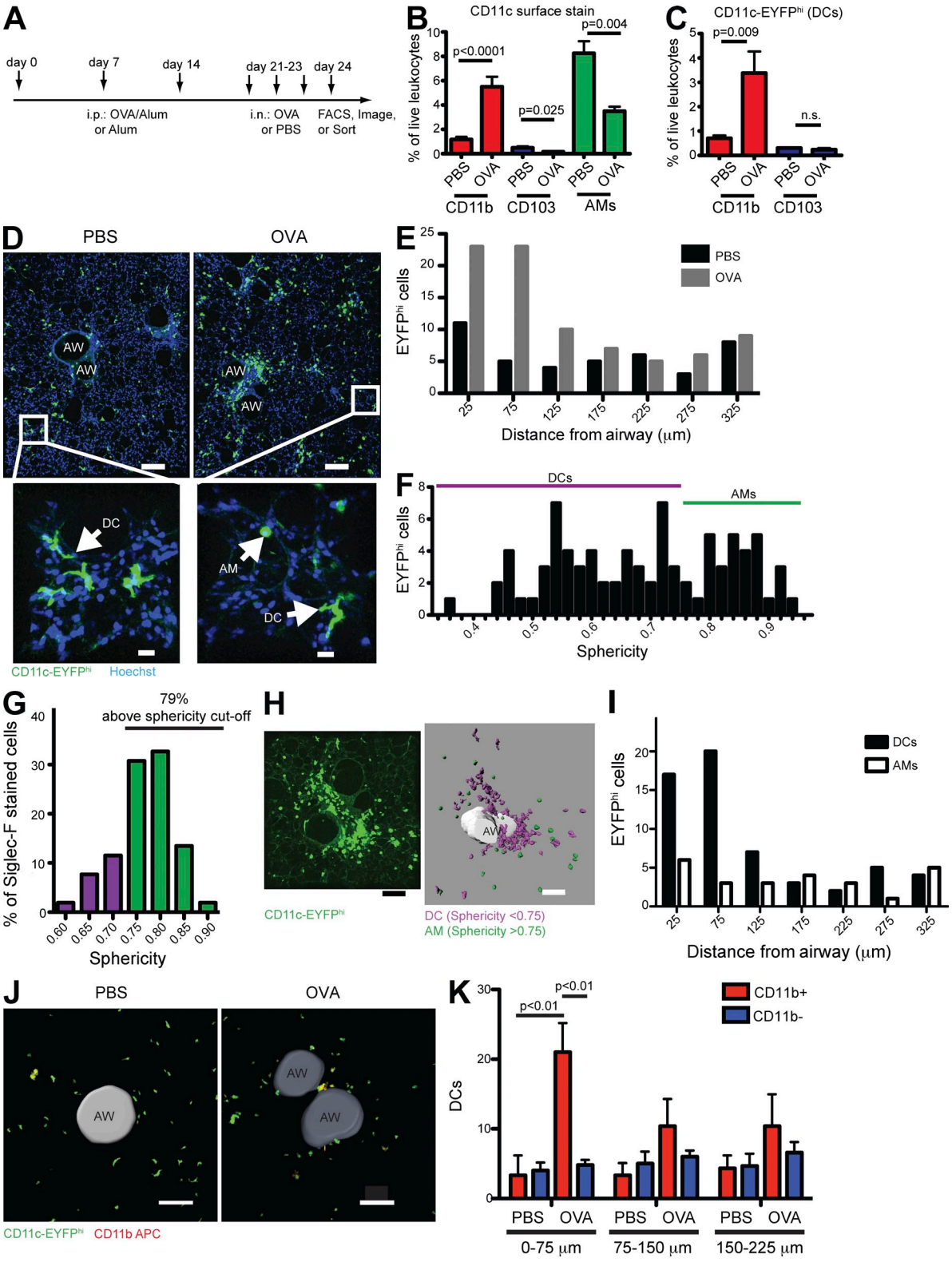

Figure 1. Specific accumulation of CD11b⁺ DCs near allergic airways. (A) Method for inducing allergic airway inflammation involving three i.p. sensitizations with OVA/alum followed by three i.n. administrations of either OVA or PBS. (B) Quantification of CD11b⁺ DCs, CD103⁺ DCs, and AMs as a percentage of live leukocytes based on CD11c surface antibody staining in lungs of PBS- and OVA-challenged mice. (C) Quantification of CD11b⁺ DC and CD103⁺ DC populations as a percentage of live leukocytes gated on CD11c-EYFP^{hi} cells in PBS- and OVA-challenged mice. (D) Large-scale three-dimensional surveys of >300-μm slices from CD11c-EYFP mice stained with Hoechst shows DC and AM distribution in PBS- and OVA-challenged mice obtained by

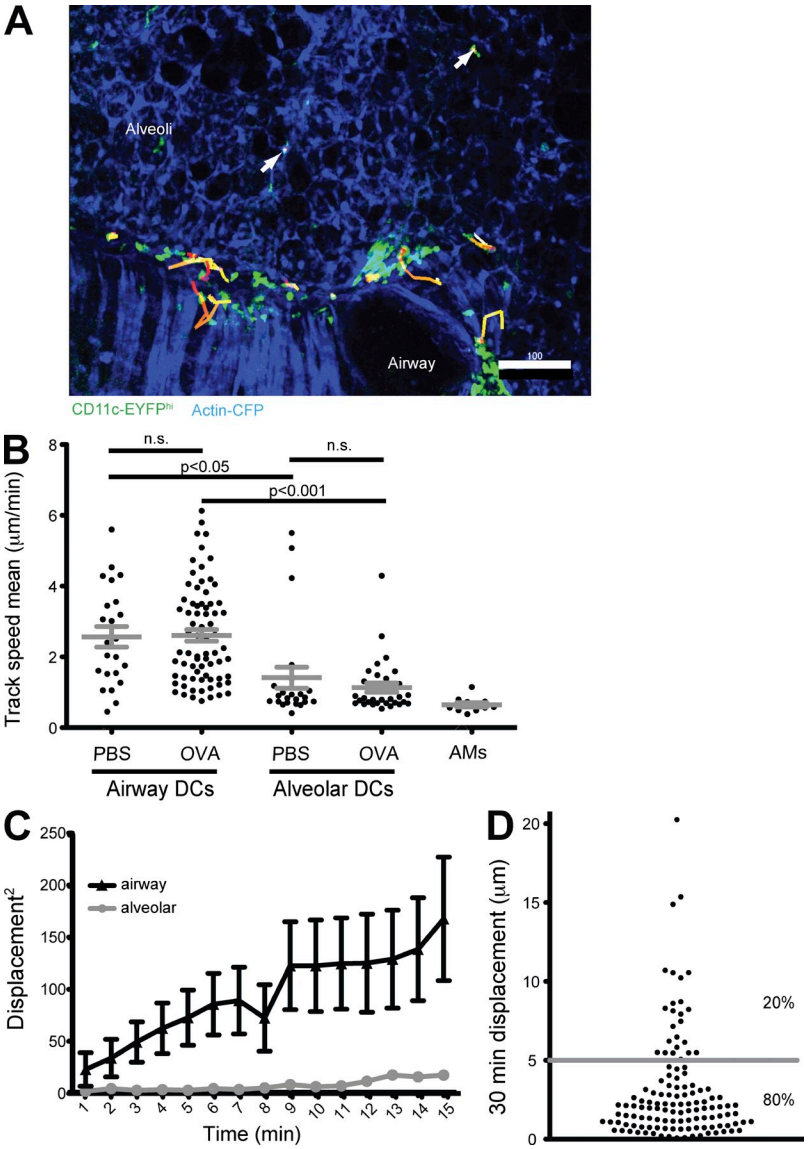

Figure 2. Airway and alveolar DCs exhibit different behaviors. (A) Detailed image with overlaid tracks of cell motility at airway surfaces and alveolar spaces over the course of 2 h. The top half of the image is mostly alveoli, whereas the bottom is mostly airway. Arrows indicate alveolar DCs. Bar, 100 µm. (B) Track speed means calculated using Imaris for CD11c-EYFP DCs and AMs separated by airway and alveolar location in PBS and OVA challenge conditions. Each dot represents one cell. Error bars represent SEM. (C) Mean squared displacements ± SE as a function of time for alveolar or airway-adjacent DCs from untreated mice. (D) 30-min displacement for alveolar DCs from OVA-challenged mice with a 5-µm cutoff, which is the diameter of one cell. Each dot represents one cell. Data are from at least three independent experiments.

of airway- and alveolar-associated DCs. This confirmed that airway DCs displace over time, whereas alveolar DCs largely do not (Fig. 2 C). However, further analysis of a large number of DCs observed over a long period of time revealed that a trafficking fraction of alveolar DCs displaced >5 µm in 30 min (Fig. 2 D).

Airway DCs are motile and send few processes through the airway

Airway DCs were motile in the airway-adjacent regions (Fig. 3 A and Video 4). However, these aggregate descriptions do not give an accurate view of individual cells. For example, we occasionally observed slow DC circling, potentially providing surveillance of a fixed area of epithelium or representing a cell under the influence of a local chemoattractant (Fig. 3 B and Video 5). By using mice expressing CFP under the actin promoter to mark all cells (Actin-CFP; Hadjantonakis et al., 2002) crossed to CD11c-EYFP, we also sought to determine whether airway DCs send processes across the epithelium, as has been shown for tracheal DCs (Hammad et al., 2009). A small fraction of DCs observed were clearly situated just below the airway epithelium while sending projections toward and possibly between the epithelial cells (Fig. 3 C and Video 6). However, only 3% of airway DCs generated processes in this way when observed over 30-min periods in PBS-treated or allergen-challenged mice (Fig. 3 D), and comparing the Actin-CFP marking, we were unable to ever observe a dendrite extend past the outermost epithelium and into the lumen.

Because previous data suggested DC sampling and/or motility was augmented by TLR stimulation in the trachea

two-photon microscopy with 910-nm excitation. Insets provide a zoomed in view of the two distinct morphologies. AW, airway. (E) Quantification of CD11c-EYFP$^+$ cells near the airways in PBS- or OVA-challenged mice. (F) Measurement of sphericity to separate DCs from AMs. AMs were defined as having a sphericity >0.75. (G) Imaris was used to make surfaces of Siglec-F$^+$ CD11c-EYFP$^+$ cells from OVA-challenged mice. The sphericity of these cells is graphed, showing that ∼80% of Siglec-F–stained AMs are captured by the sphericity measurement. (H) Color coding of localization based on sphericity with bulk CD11c-EYFP data shown on the left and subdivided data (DCs, purple; AMs, green; airway, white) on the right from an OVA-challenged mouse. (I) Images were subdivided by sphericity to determine whether DCs or AMs account for the accumulation within 75 µm of the airway after OVA challenge. (J) Example images from CD11c-EYFP sections (gated on EYFP$^+$ sphericity <0.75) stained with CD11b APC. Bars: (D [top] and H) 100 µm; (D, bottom) 10 µm; (J) 150 µm. (K) Quantification of CD11b$^+$ and CD11b$^-$ DC distance from the nearest airway for PBS- and OVA-challenged mice. (B, C, and K) Error bars represent SEM. Graphs represent at least five mice per group from at least three independent experiments. Images are representative data from at least three independent experiments.

(Hammad et al., 2009) and gut (Chieppa et al., 2006), lung sections were treated with LPS to measure changes in DC behavior. Up to 3 h after treatment, airway DC speed remained unchanged (Fig. 3 E), and we observed no change in sampling behavior or frequency (not depicted). Because the previous findings of changes in DC behavior were mediated by epithelial TLR4, it was tempting to hypothesize that, in comparison, the lung epithelium may not induce the requisite changes to augment DC scanning. Staining of collagenase-digested lung and trachea confirmed that the population of TLR4-expressing cells in the trachea was 10 times that of the lung, possibly accounting for differences in DC responses at these sites (not depicted). We thus conclude that, within this short time scale, before LPS induced major lung injury, DC surveillance in the airway remained confined to the interstitium.

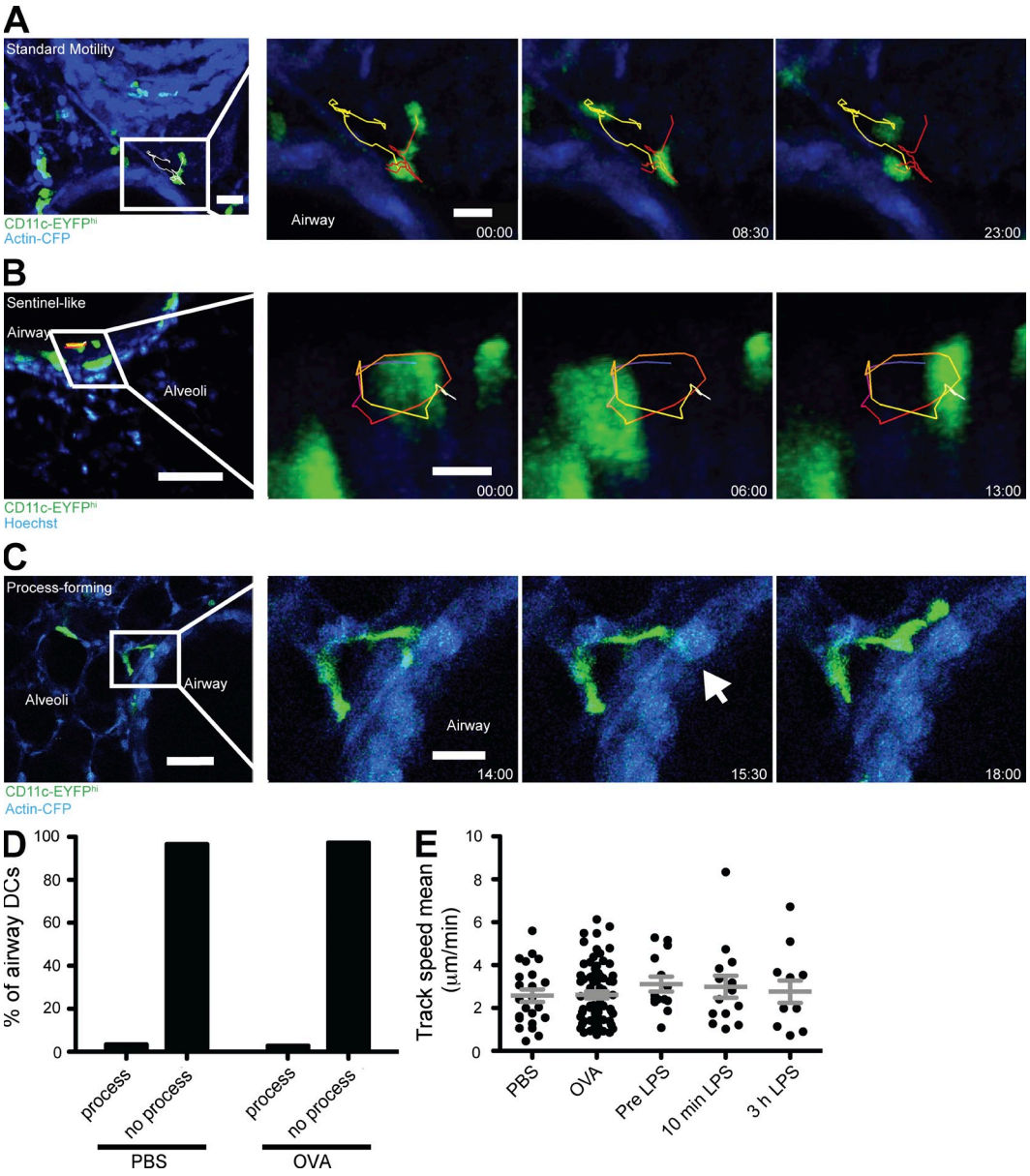

Figure 3. Airway DCs are motile but send few processes through the epithelium. (A) Standard motility of airway-adjacent DCs. Entire field for orientation (left) followed by zoomed images from relevant regions collected at the indicated times. (B) Sentinel-like motility of CD11c-EYFP cells on the inner surface of an airway obtained using two-photon microscopy and rendered in Imaris. (A and B) Yellow and red lines indicate tracks of two airway-adjacent DCs over a 30-min time lapse. (C) Process-forming DCs marked by CD11c-EYFP in Actin-CFP background. Process to probe epithelium is indicated by an arrow. Bars: (A, left) 25 µm; (A and C, right) 15 µm; (B and C, left) 50 µm; (B, right) 10 µm. Time stamps are shown in minutes/seconds. (D) Quantification of processes from airway DCs across airway epithelium in PBS- or OVA-challenged mice. (E) Track speed means of airway DCs from PBS- or OVA-challenged mice, before LPS treatment or after 10 min or 3 h of LPS treatment. Each dot represents one cell. Error bars represent SEM. Images are representative images from >12 mice per group. Quantification of track speed means are combined data from three separate experiments.

Alveolar DCs send dendrites into airspace

Although DC center of mass motility was limited in the alveoli (Fig. 2 C), analysis of time lapses demonstrated that the dendrites of these cells were quite active. This was evident under steady-state as well as for allergen-challenged DCs (allergen challenged: Fig. 4 A and Video 7). As with airway DCs, intercrosses with Actin-CFP mice provided sufficient contrast to analyze whether dendrites were transepithelial, and in contrast with airway DCs, alveolar DCs demonstrated extending and retracting dendrites moving along the mucosal face of alveolar epithelial cells (unchallenged mouse: Fig. 4 B and Video 8). DCs extending and retracting multiple dendrites were also observed to extend into multiple alveoli at the same time. Surprisingly, quantification of both the number of extended dendrites and the total surface area (a value that increases as dendritic projections increase in number or size) shows no difference in the phenotype of cells after control or allergen challenge (Fig. 4, C and D). As was shown in airway cell behavior, treatment with LPS did not increase DC motility (Fig. 4 E). The efficacy of our LPS was shown by its ability to induce 48-h lung injury in experiments using the same reagent (not depicted).

DCs are very responsive to tissue stressors, and so we considered it possible that our section method may have induced behaviors in these cells that are not present in normal, intact lung. As we also wished to broadly test the validity of the slice model for supporting normal lymphocyte behaviors, we adopted a newly described intravital live imaging method (Looney et al., 2011). Alveolar projections along the mucosal face of alveolar epithelial cells in CD11c-EYFP Actin-CFP lungs were again observed in control conditions (Fig. 4 F and Video 9). The number of projections was both similar to that observed using the slice method and was also conserved between control and allergen challenge conditions (Fig. 4 G). Because AMs reside in the alveolar airspace, it is possible that filling the lung with agarose could impede their motility; however, the live imaging system also showed that AMs in mechanically ventilated lungs also demonstrated very little migration (Fig. 4 H).

Alveolar but not airway DCs sample antigen

The position and morphological characteristics of DCs in the alveoli were consistent with an active role as phagocytes in this setting. We modified our OVA challenge protocol to include the intranasal (i.n.) administration of both labeled OVA (to prime immune responses) and highly fluorescent 1-µm polystyrene beads at the last i.n. challenge before sacrifice to assess their ability to directly capture model antigens from the airspace (Fig. 5 A). When assessed within 1 h of antigen administration, we were able to directly observe the dendrites capturing the microspheres and retracting, bringing the antigen into the cell body (Fig. 5 B and Video 10). In this example, a subsequent dendrite projecting from the same region of the DC that did not carry the bead outward again during this projection indicated that the bead had been transported into the cell body. Three-dimensional rendering confirmed that the bead was within the volume of the labeled cell (not depicted). As noted previously, we only observed this uptake in alveolar DCs (Fig. 4 B) but have not observed similar transepithelial bead capture by airway-adjacent DCs (Fig. 3 D). In contrast, when we imaged lungs 24 h after bead inhalation, we now also observed motile DCs within the nonalveolar interstitium, bearing beads near the airways (Fig. 5 C and Video 11). This sequence of events strongly suggests a predominance of at least initial uptake in the alveoli followed by release and trafficking of DCs into the airway-adjacent region.

To quantify these dynamics from images, we gated our analysis upon DCs and determined the percentage of airway-adjacent DCs (defined as being 0–75 µm from the airway border) versus alveolar DCs (>75 µm from the airway border) that were carrying model particulate antigen immediately after and 48 h after bead inhalation (Fig. 5, D and E). Because of the architecture of the lung, it is impossible to objectively define an airway-adjacent region that completely excludes alveoli. The arbitrary 75-µm border was chosen to prevent bias in image analysis. We expressed the percentage of bead-bearing DCs as a normalized percentage (see Materials and methods), and we only analyzed data that had bead densities within twofold ranges to minimize any effects caused by the overall density of beads (not depicted). As assessed in this way, the percentage of alveolar DCs with antigen was 10% at 2 h after inhalation, and this was very similar with allergen challenge (12%). The percentage of DCs bearing beads in alveoli increased at 48 h to 39%, suggesting additional alveolar uptake and retention of some antigen-bearing cells. Again, there was no statistically significant difference between the PBS- and allergen-challenged mice in terms of rate of uptake, which is consistent with our observations of their scanning behaviors.

In contrast, DCs within 75 µm of airways at 2 h in control and allergen challenge were 6% and 0% bead positive, respectively (Fig. 5 E). This suggested a significant defect in the ability of these cells to ingest antigens, and we noted that the majority of the few cells that became bead positive likely had access to alveoli that lay within this cutoff distance. In PBS-treated control mice, this level of bead-bearing DCs in the control-treated condition remained low (3%) 48 h later, showing that few antigen-bearing cells accumulated there over continuous exposure. However, in OVA allergen–challenged animals, DCs bearing particles represented 18% of airway-adjacent DCs by 48 h (Fig. 5, D and E). One explanation for this profound rise would be that DCs that ingested antigen in the alveoli and migrated toward the airway were specifically recruited and retained there in allergen challenge conditions. Alternatively, the airway DCs may capture antigens more efficiently over time and then stay within that region. Although we rarely observed airway DCs to send processes across the epithelium more consistent with the former hypothesis, we sought to address the dynamics of antigen partitioning to address these possibilities.

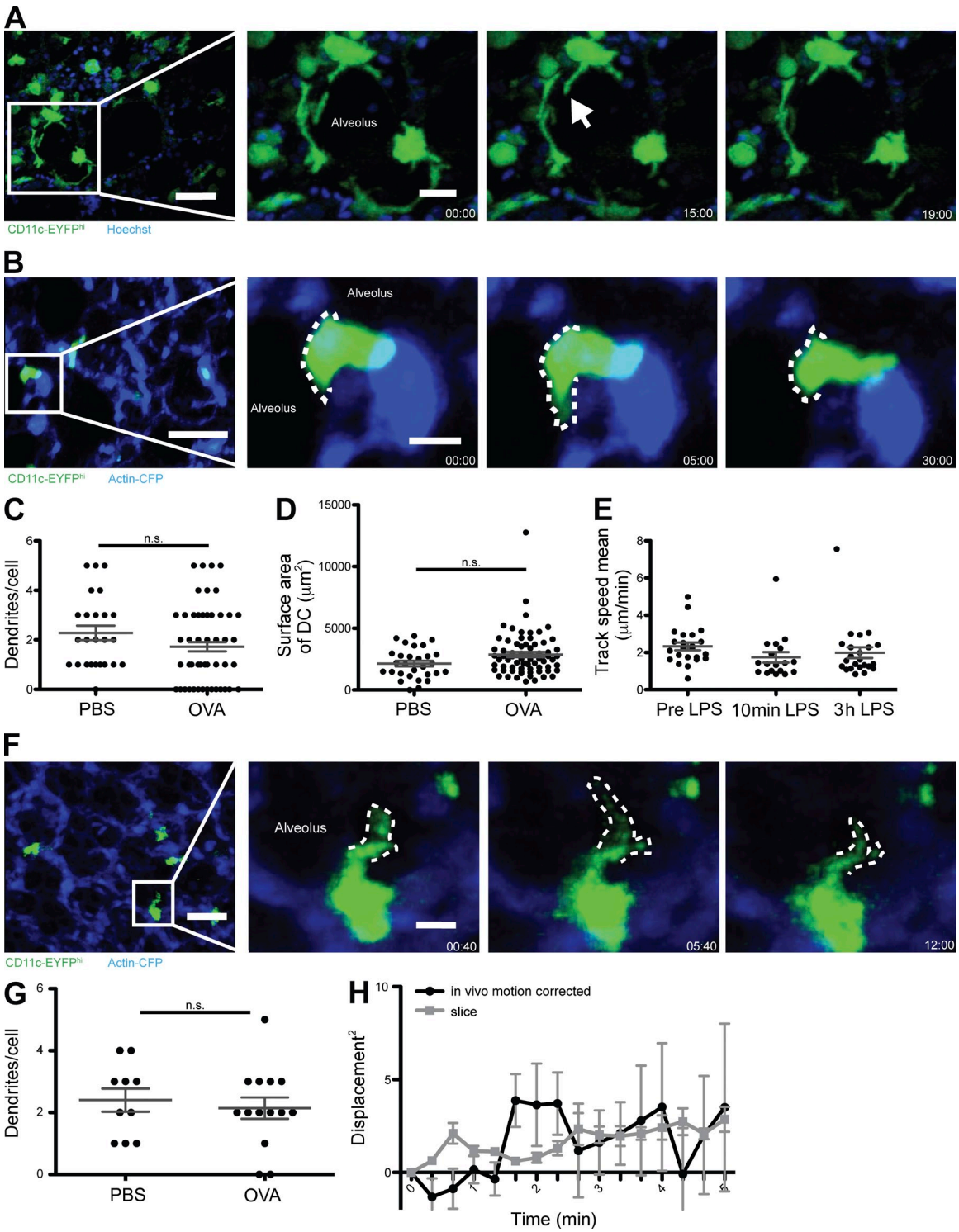

Figure 4. DCs sweep the alveolar air space using transepithelial dendrites. (A) Motility of CD11c-EYFP DCs in the alveolus of an OVA-challenged mouse stained with Hoechst. The arrow indicates an extended dendrite. (B) Alveolar motility of a CD11c-EYFP DC in a PBS-treated Actin-CFP mouse. (C) Quantification of dendrite numbers per alveolar DC for PBS- and OVA-challenged lungs. (D) Surface area of alveolar DCs from PBS- and OVA-challenged mice calculated using the isosurface tool in Imaris. (E) Track speed means of alveolar DCs before LPS treatment or after 10 min or 3 h of LPS treatment. (F) Intravital in vivo motility of a CD11c-EYFP DC in the alveolus of an Actin-CFP mouse that is anesthetized, ventilated, and imaged with two-photon microscopy. (B and F) Dotted lines trace the dendrite surface. Bars: (A, B, and F, left) 50 µm; (A and B, right) 20 µm; (F, right) 10 µm. (G) Quantification of intravital in vivo dendrite numbers per alveolar DC for PBS- and OVA-challenged lungs. (H) Mean squared displacements as a function of time for AMs from in vivo lungs corrected for breathing artifacts with type II epithelial cells versus sectioned lungs. (C–E, G, and H) Error bars represent SEM. Images are representative images from >12 mice per group for slice and 4 mice per group for live imaging. Quantification of dendrites, surface area, and track speed means are combined data from three separate experiments.

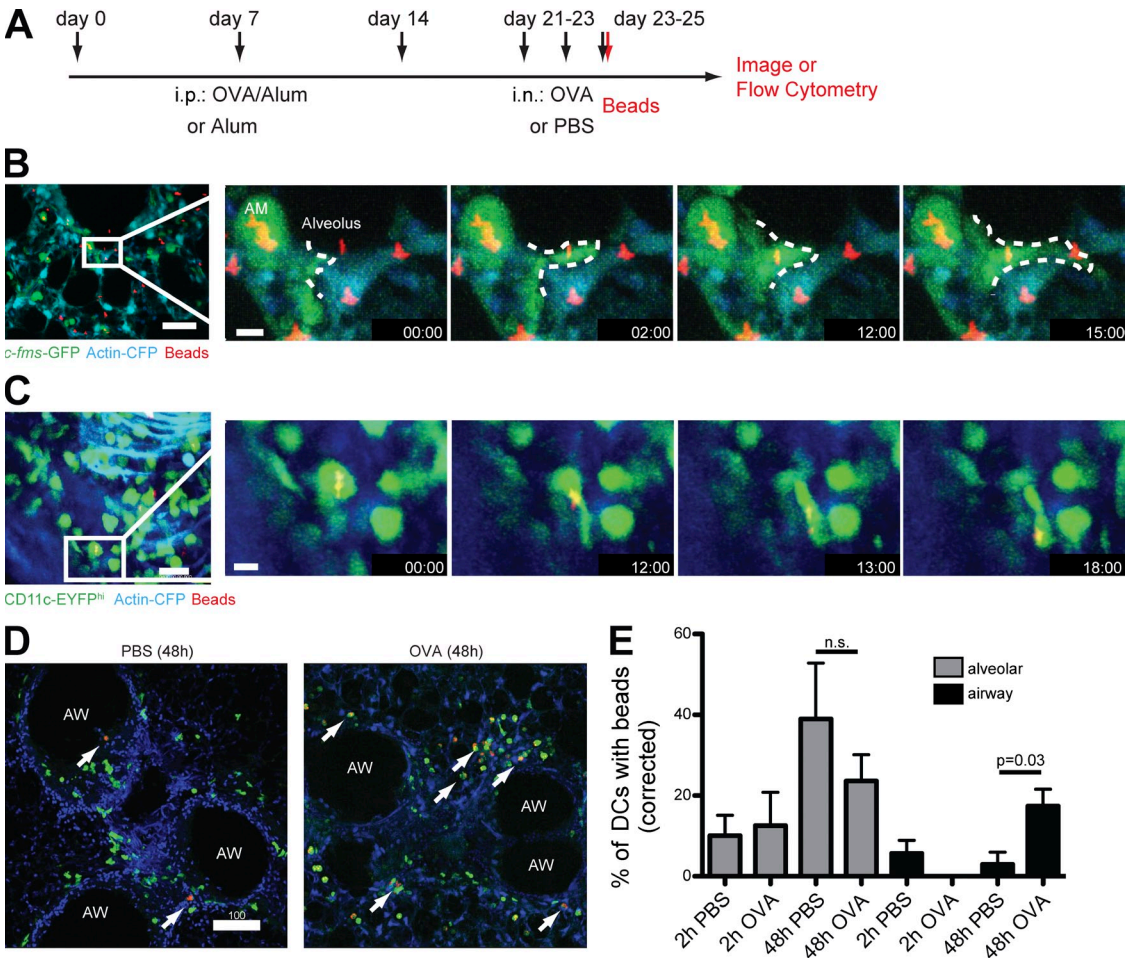

Figure 5. DCs directly phagocytose inhaled antigens and accumulate model antigen in airway-adjacent regions. (A) Scheme for allergen challenge includes three i.p. injections of OVA/alum and three i.n. instillations of OVA (black arrows) followed by an i.n. instillation of beads (red arrow). (B) Stills of a video from a *c-fms*–EGFP, Actin-CFP mouse 1 h after i.n. instillation with 1-µm fluorescent polystyrene beads. Note extension, uptake, retraction, and reextension of the indicated DC. Also note the round AM to the left of the DC, within the alveolus. Dotted lines trace the dendrite surface. (C) Migration of CD11c-EYFP cells just below the surface of an airway of an OVA-treated lung stained with Hoechst (blue) 24 h after bead inhalation. (D) Representative image of airway (AW)-associated, antigen-bearing DCs in PBS- and OVA allergen–challenged mice. Arrows indicate DCs with beads. Bars: (B and C, left) 50 µm; (B, right) 10 µm; (C, right) 20 µm; (D) 100 µm. (E) Quantification of proportion of alveolar and airway-associated DCs that contain beads immediately after and 48 h after bead inhalation corrected for the total number of beads inhaled. Error bars represent SEM. All images are representative of at least four mice per group from four independent experiments. Quantifications include data from four independent experiments.

We therefore adopted a system where PBS- or OVA-challenged mice were given two rounds of beads with a 2-d interval between to compare immediate uptake with equilibrated pools. Mice received blue beads i.n. after their third challenge (day 23; 2-d equilibration) and red beads 48 h later (day 25; immediate uptake; Fig. 6 A). Mice were then immediately analyzed by imaging to determine where each pool of beads was localized. Fig. 6 B shows airway regions in control and OVA-challenged mice and demonstrates the near 1:1 accumulation of equilibrated (blue) and immediate (red) beads in control lungs but an increased prevalence of the blue equilibrated beads (13:5 ratio blue/red in the images) in allergic lungs. Quantification of the ratios of equilibrated and immediate beads by region demonstrates that airways favor equilibrated beads over immediate beads most prominently in allergen-challenged airways (Fig. 6, B and C). In control lungs, there was no specific retention of the equilibrated beads at either site.

In Fig. 1, we demonstrated that the majority of DCs that accumulate near the airways are $CD11b^+$. However, several studies have shown that $CD103^+$ DCs, which occur in very small numbers in the lung after allergen challenge, are important for traffic to the draining LN in other disease models (Jakubzick et al., 2008a; Lukens et al., 2009; Desch et al., 2011). We sought to independently confirm that the retention we observed was specific to the lung airway in comparison with the LNs. For this, mice inhaled a single color of bead, and mediastinal LNs were analyzed after 48 h. In contrast to the airway region, $CD11b^+$, $CD103^+$, and LN-resident DCs were present in similar proportions in the LN

of PBS- and allergen-challenged mice (Fig. 6 D), showing that under "sterile" allergen challenge (i.e., without overt pathogen), these cells continue to populate the draining LN with similar dynamics. When all beads in the LNs at 48 h were enumerated by flow cytometry and assigned using surface markers to the DC subset that bore them, CD103 DCs were represented 45% out of proportion to their frequency among all DCs (20%), consistent with a more active trafficking role (Fig. 6 E). In contrast with the airway, all three subsets of lung-draining DCs bore model antigen at similar frequencies under control versus challenge conditions. This therefore suggests that allergic lungs specifically retain antigen-bearing DCs within the airway-adjacent region without evidently altering LN trafficking. Although allergens are frequently particulate and therefore this form of uptake is possibly most relevant, we also compared these populations for uptake of a soluble fluorescent OVA conjugate via FACS. Although percentages of cells were largely the same and percentages among phagocytes again mostly mirrored relative abundance, CD11b$^+$ DCs were notably better at soluble antigen uptake (not depicted). This may be a result of the enhanced access of this form of antigen to permeate the subairway region coupled with the overall higher frequency of this cell type (Fig. 1).

DC–T cell interactions occur near allergic airways

The use of OVA as a model allergen permitted us to study the dynamics of retained DCs relative to antigen-specific T cells and the degree to which interactions might be confined to this site. By transferring naive, CD2-RFP–labeled OTII T cells (Veiga-Fernandes et al., 2007) before a single i.p. allergen sensitization, these antigen-specific cells were expanded. They were subsequently recruited to the lung and mediastinal LN during the allergen challenge phase

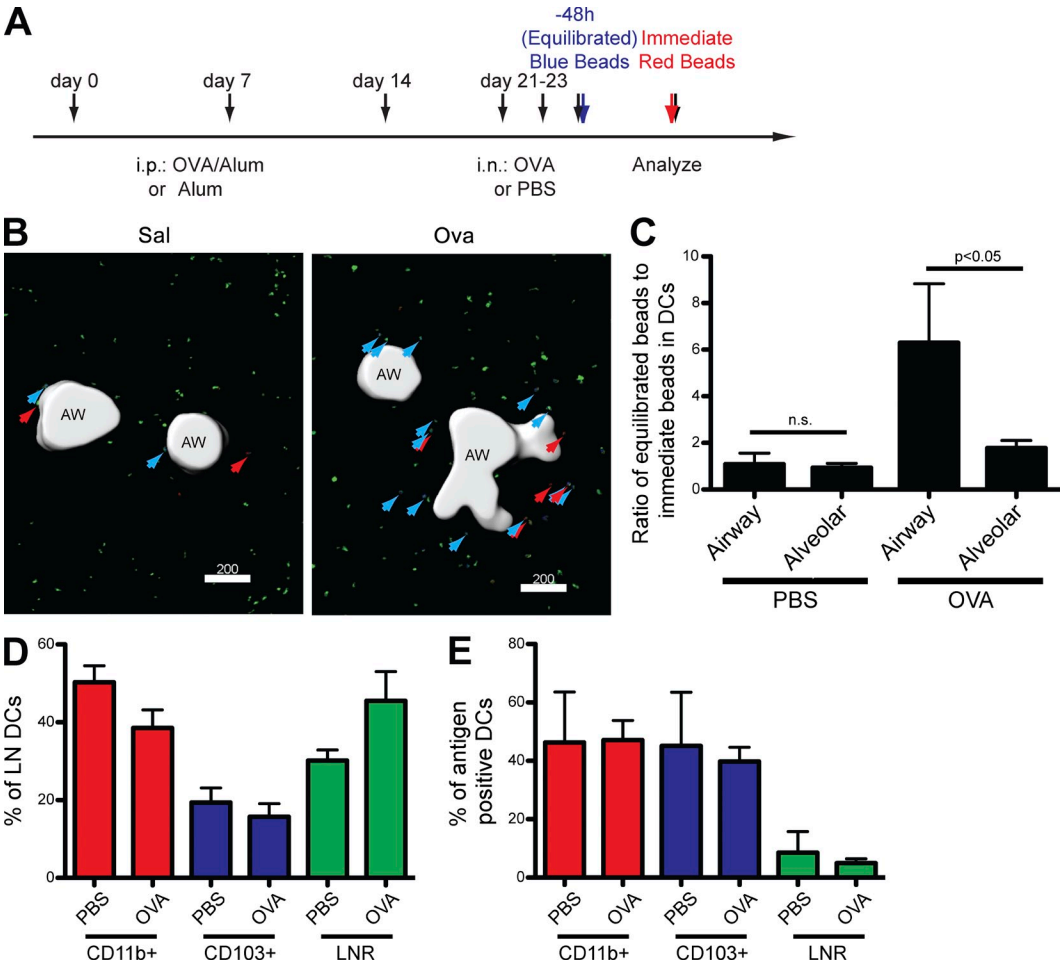

Figure 6. DCs carry model antigen to airway-adjacent regions as well as LNs. (A) Scheme for allergen challenge includes three i.p. injections of OVA/alum and three i.n. instillations of OVA or PBS (black arrows), an i.n. instillation of red beads (red arrow), and an i.n. instillation of blue beads (blue arrow) to dissect uptake versus trafficking. (B) Example images of beads in CD11c-EYFP DCs. Arrows indicate example beads in DCs. Bars, 200 µm. (C) Quantification of beads in CD11c-EYFP DCs yielded the ratio of equilibrated (beads inhaled 48 h before analysis) to immediate (beads inhaled directly before analysis). The airway region is defined as 75 µm from the inner airway surface. (D) CD103, CD11b, and LN-resident (LNR) DC populations were compared by FACS after PBS or OVA challenge. (E) The phenotype of DCs carrying model antigen to the LN was analyzed by FACS 48 h after bead inhalation. (C–E) Error bars represent SEM. All data represents at least eight mice per group from at least five independent experiments.

(not depicted). Antigen-specific T cells accumulated near airways after allergen challenge and interacted with airway-adjacent DCs (Fig. 7, A and B; and Video 12). We observed T cells that move from one DC to another; however, on average, airway-adjacent T cells were in contact with at least one DC for >90% of the time observed, thus providing ample opportunities for continued stimulation. In contrast, the few T cells that were present near alveoli were very rarely in contact with DCs (Fig. 7 C). We then adopted preactivated OTII or control SMARTA (LCMV gp specific) T cells during the challenge period to compare activities of allergen-specific and nonspecific cells. Interestingly,

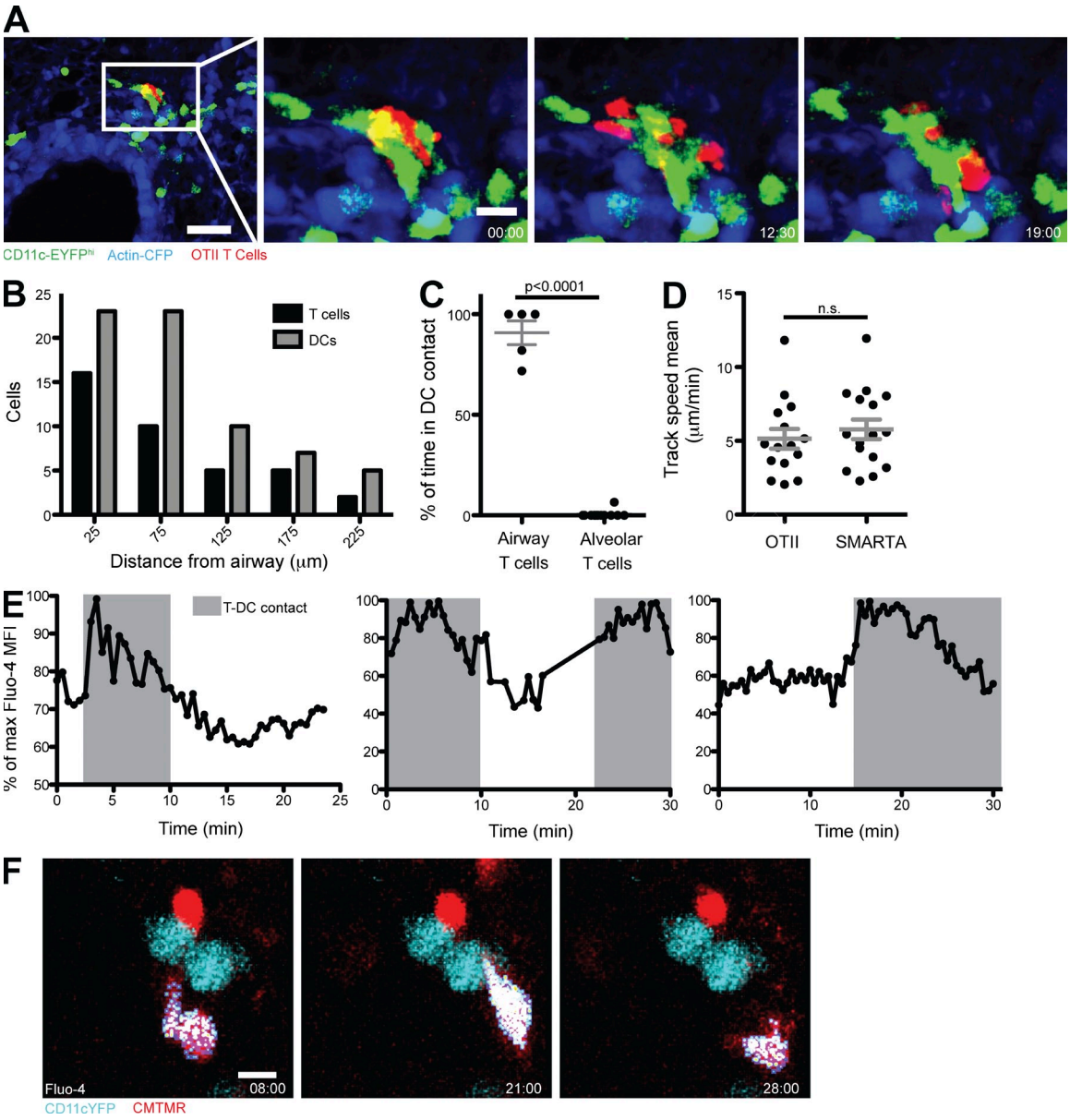

Figure 7. Activated T cells interact with airway-adjacent DCs. (A) Interactions of T cells (red) and DCs (green) illustrated by a time course showing T cells swarming over the surface of multiple DCs but always remaining in contact with at least one. (B) OTII T cell accumulation within 75 μm of a representative airway compared with DC accumulation within the same area in an OVA-challenged mouse. (C) Percent duration of a 30-min video that OTII T cells were in contact with at least one DC in either the airway or alveolar region. (D) Track speed means for previously activated antigen-specific (OTII) or nonspecific (SMARTA) airway T cells. (C and D) Error bars represent SEM. (E) Activated antigen-specific (OTII) T cells were stained with CMTMR and Fluo-4 and transferred into OVA-challenged CD11c-EYFP mice 6 h before imaging. Percentage of maximum mean fluorescence intensity (MFI) of Fluo-4 in previously activated T cells. Gray background indicates the time that T cells are in contact with a DC. Each panel represents one cell. (F) Transferred T cell stained with CMTMR and Fluo-4 (gated on the CMTMR signal of the cell, pseudocolored) moves toward an airway, transiently interacting with a DC (teal) on the way. Bars: (A, left) 50 μm; (A, right) 15 μm; (F) 10 μm. Time stamps are shown in minutes/seconds. Images and quantification are representative of at least three mice per group from at least two independent experiments.

velocities of previously activated airway-associated antigen-specific OTII T cells (mean velocity of 5.1 µm/min) were similar to the previously activated nonspecific SMARTA T cells (mean velocity of 5.7 µm/min; Fig. 7 D). Because previously activated cells are recruited to this space, these data imply that this airway region serves as a meeting ground where recently activated T cells may meet up with DCs that recently sampled the alveolar airspace and that neither entry nor motility are antigen-regulated. These data suggest that the airway-adjacent region attracts activated T cells and antigen-loaded DCs in allergic lung disease where they are more likely to interact. To determine whether the serial interactions of these previously activated cells result in activation (as measured by calcium flux), activated OTII cells were labeled with Fluo-4 and CMTMR before transfer. This demonstrated that allergen-specific T cells signal upon even these transient interactions with airway-associated DCs (Fig. 7, E and F; and Video 13). This data highlights that T cells and DCs are dynamically engaging in contact rather than assembling as stable static structures, giving rise to a continuously evolving microenvironment that affects the ongoing immune response.

DISCUSSION

An important finding of this work is the regional segregation of DC behaviors resulting in separated antigen surveillance and presentation within the lung despite no changes in sampling behavior after allergen challenge. Importantly, the behavior of DCs in the lung is not well represented by what was previously observed in the trachea, which has been the site of choice for analysis of DC phenotype, morphology, and dynamics (Lambrecht et al., 1998; Jahnsen et al., 2006). The alveolar regions of lung favor uptake, with almost every DC visualized having dendrites into the surfactant layer. In contrast, the airway is a site of antigen-bearing DC accumulation and T cell activation.

Alveoli: A competitive landscape for antigen capture

AMs, as professional phagocytes, account for ∼95% of BAL leukocytes and are therefore considered as the sentinel phagocytic cells of the respiratory tract (Martin and Frevert, 2005). Yet DCs appear to be the primary cells to carry antigens for presentation to T cells, particularly in asthma (McWilliam et al., 1996; Vermaelen et al., 2001; van Rijt et al., 2005). Our study generates a vivid picture of the varied uptake strategies of these cell types. In both intravital and lung-slice imaging, AMs are immotile within alveoli and likely require antigens to come to them. In contrast, alveolar DCs actively scan and take up antigens as they "sweep" the alveolar air space. Both of these cell types likely benefit from the surfactant layer providing a medium for the collection of inhaled particles or pathogens, reducing the distance DCs must travel into the alveolus to sample its contents. The uptake capacity of alveolar DCs was clearly shown by the active uptake of inhaled particulate antigen from the alveolar air space.

A further competition likely occurs between DC subsets. Recent studies have emphasized the distinction between $CD103^+$ and $CD11b^+$ DCs in traffic and presentation capacities within the barrier tissues of the body. In the lung, $CD103^+$ DCs have been shown to play an important role in immunity to viral infection (Lukens et al., 2009) and carry apoptotic cell debris to the draining LN (Desch et al., 2011). The location and sampling behaviors of these DCs have not been reported in the lung nor have changes during nonpathogenic allergen responses been compared. In this study, we describe that the few $CD103^+$ DCs in the lung are distributed throughout the tissue, whereas $CD11b^+$ DCs are present throughout the lung and accumulate near the airways after allergen challenge. The presence of $CD11b^+$ DCs in greater numbers and near the airways suggests the importance of $CD11b^+$ DCs instead of $CD103^+$ DCs in the ongoing pathogenic immune responses that are associated with asthma.

Because recruited $CD11b^+$ DCs have been proposed to arise from inflammatory monocytes (Lambrecht and Hammad, 2009), it is possible that recruited monocytes also compete for antigen within the lung. Monocytes might be predicted to extravasate into the interstitium or into the surfactant layer. There, they may ultimately differentiate into one of the other DC cell types and contribute to the accumulations we observe. The role that they play as phagocytes before such differentiation is not yet clear but may reveal additional mechanisms and sites for antigen uptake.

Despite having a very low mean speed, analysis of many cells identified a motile population of alveolar DCs. These slow but migratory DCs likely contribute to antigen trafficking and the accumulation of DCs at the airway after allergen challenge. Although we did not discern directional migration toward airways for DCs located >75 µm from the airways (unpublished data), those located near the airways were largely retained in the clusters there. This would suggest two steps in the recruitment of DCs to the airway after allergen challenge, one that leads to release of DCs in the alveoli and a second, likely chemokine, that captures the cells when they are sufficiently close to the chemokine source. Future studies identifying the factors that elicit these cells to leave their positions in the tissue or those that capture them into the DC clusters may allow for the process to be perturbed for therapeutic means.

Regional segregation of antigen surveillance and presentation in the lung

Cellular projections into airspace have been reported across human nasal mucosa of allergic rhinitis in situ, where dendrites penetrate beyond well-developed epithelial tight junctions (Takano et al., 2005). Similar findings were reported in a rat tracheal model in which 1–5% of intraepithelial DCs were observed to extend projections into the airway lumen, both under steady-state conditions and during inflammation (Jahnsen et al., 2006). The airways, fundamental sites of asthma responses, were notably sparse with these projections. And, although we routinely confirmed that our protocol reproducibly generated eosinophilia and airway hypersensitivity (unpublished data), it did not lead to increased dendritic probing at the airway.

This highlights the differences between nasal epithelium, trachea, large airways, and alveoli.

Another level of regional difference is evident because dendritic projections in the alveoli are largely independent of allergen or TLR challenge. This differs from the report of transepithelial surveillance by DCs in the gut where TLR stimulation leads to increased surveillance (Chieppa et al., 2006). Although fixed tracheal sections have demonstrated that DCs are capable of making projections there (Jahnsen et al., 2006), live imaging of TLR-dependent changes have focused on increased motility of DCs in subepithelial regions. This increased mobilization was shown to be dictated by TLR signaling in epithelial cells rather than in the DCs themselves (Lambrecht and Hammad, 2009). As we demonstrate, TLR4 expression is vastly different between trachea and lung. It is therefore likely that regional differences in the epithelia play a key role in determining responses to inhaled material at distinct sites.

One possible model from these data is that pathogenic microbes detected in the trachea or nasal mucosa could generate a danger response leading to DC uptake, trafficking, and generation of active immune responses. In contrast, the distinct absence of these projections in airways may ultimately protect the delicate and critical conducting airways from all but the most dangerous pathogens that make it deep into the lung or breach the epithelium. At the deepest levels, alveolar DCs may exist to sample for fulminate bacterial or helminth infections. These DCs may be capable of both priming a response in the LN and, through an as-yet-undiscovered mechanism, be successfully retained to boost effector responses near the affected airway. Asthma, in this model, may result from the over-retention of antigen-bearing DCs near the airways, which activate the already-primed Th2 T cells from the circulation.

Regional retention of $CD11b^+$ DCs near airways is the basis for a new model DC contribution to the pathogenesis of asthma (unpublished data). LN $CD11b^+$ DCs have been shown to play an important role in CD4 T cell priming (Jakubzick et al., 2008a). Activated T cells are recruited to the areas of DC accumulation and swarm along the surface of these DCs, without arresting to signal. Calcium fluxes observed in these motile airway-associated T cells likely reflect the lower activation threshold of previously activated T cells, making the airway a site for antigen-specific repriming. Although these data point to DC repriming of CD4 T cells, there may be additional maturation of DCs that is a consequence of this interaction. Indeed, we note that DCs from allergen-challenged lungs have higher class II expression. Although methods do not exist to test this prediction, it is interesting to speculate that the T–APC clusters we visualize may also represent the precursor to bronchus-associated lymphoid tissue (BALT) and that similar foci may form at these sites in response to infections.

Dynamic imaging in the lung

Two-photon imaging has been successfully applied to immune cells in multiple sites including LNs, spleen, brain, and gut. This study provides insight into the nature of immune cell dynamics in lung airways and alveoli. Although the lung slice model (Bergner and Sanderson, 2003) has been previously established as a suitable model for studying smooth muscle contractility, it was not established that this slice method would preserve the behaviors of immune cells. Our demonstration that DCs, whose behaviors are thought to be very sensitive to tissue damage, function similarly in the slice model as compared with intravital imaging provides validation for its use in future experiments. Future investigators will want to be wary of the pitfalls of the slice model that include cell death near the cut site and the absence of incoming cells via the blood or egress via the lymph. However, the method avoids challenging surgeries and tissue stabilization procedures (Looney et al., 2011), provides an ideal mechanism by which to perfuse in reagents or cells, is amenable to higher throughput, and allows observation of airways distant from the lung surface. A similar side by side comparison of T cell motility in excised LN as compared with intravital LN imaging (Miller et al., 2002, 2003) has provided the basis for many exceptional studies using the organ model. It will be important for each subsequent study to assess the validity of observations in slice models using criterion specific to the questions being addressed.

Further implications for lung immunity

It is important to note that pathogens may compound and alter the DC recruitment that we observed with allergen challenge. For example, increases in DC number in the lung, particularly along the trachea, are also seen in viral infection (McWilliam et al., 1996). Infection with *Mycoplasma pulmonis* leads to increases in lung DCs even more pronounced than that seen after acute allergen challenge (unpublished data). Bacterial, viral, and mycoplasma infections have also been associated with exacerbations of asthma (Kraft et al., 1998; Martin et al., 2001; Tan, 2005), and lung DCs have been shown to stimulate T cells after viral infection (Hamilton-Easton and Eichelberger, 1995).

One interpretation of these previous findings in the context of our observations is that a pathogen-mediated accumulation of DCs in the lung results in more antigen uptake and presentation by these inflammatory DCs within the lung. Pathogens can also cause an increase in DC activation state caused by TLR signaling mediated by the pathogen and thus exacerbate responses to allergens. It remains to be determined whether these multiple insults might also lead to variations in the site and timing of interactions between antigen-loaded DCs and naive or effector T cells. Specifically, in settings in which different DC subsets appear to play dominant roles (i.e., $CD103^+$ in viral and $CD11b^+$ in asthma responses), it will be important to understand which cells dominate and how they affect the subsequent responses. The interactions between T cells and DCs seen in peri-airway regions likely allow for adaptive immune responses to allergens to occur quickly, without the need for cells to traffic to the draining LN. These data correlate with the late phase of the asthma

response, which is an adaptive response but begins only 8 h after allergen inhalation (Wenzel et al., 2007).

This study sheds light on several steps in the immune response to an allergen that may be targeted for therapy. Antigen uptake, DC accumulation, and T–DC interactions occur sequentially and may therefore be targeting separately or concomitantly for effective therapy. Because we have shown the importance of alveolar uptake, it is important to consider the ability of therapeutic agents to reach the distal portions of the lung. Future studies should address possible mechanisms to target antigen away from $CD11b^+$ DCs and toward a possibly tolerogenic pathway. Our data examines a "naked" model antigen, but antigens coated with biologically relevant molecules may represent a prospect for therapy if they can be targeted away from airway-retained populations. Conversely, targeting depleting agents to these cells may also block the pathogenic immune response. In that respect, a previous study has shown preferential uptake of bacteria by AMs (Pedroza-González et al., 2004). More study is also required to address the factors that lead to the accumulation of antigen-bearing DCs and previously activated T cells in the airway-adjacent region. Blocking antigen traffic and/or T cell recruitment may prevent productive T cell activation and delay or prevent the onset of severe symptoms at the airway.

MATERIALS AND METHODS

Mice. All mice were bred and housed in specific pathogen–free housing and in accordance with the guidelines of the Laboratory Animal Resource Center of the University of California, San Francisco (San Francisco, California). All mice were C57BL/6 background. CD11c-EYFP (Lindquist et al., 2004) transgenic reporter mice were provided by M. Nussenzweig (The Rockefeller University, New York, NY), and *c-fms*–EGFP transgenic mice (Sasmono et al., 2003) were provided by Z. Werb (University of California, San Francisco). Both CD11c-EYFP and *c-fms*–EGFP mice were crossed to Actin-CFP mice (Hadjantonakis et al., 2002) obtained from I. Weissman (Stanford University, Stanford, CA). OTII TCR transgenic mice were obtained from the Jackson Laboratory, and CD2-RFP (Veiga-Fernandes et al., 2007) mice were a gift of M. Coles (University of York, York, England, UK). Approval for the use of mice in this study was obtained from the Institutional Animal Care and Use Committee of the University of California, San Francisco.

Antibodies and flow cytometry. Antibodies used include CD45 APC-Cy7 (30-F11; BD), CD4 A647 (GK1.5; UCSF Hybridoma Core), MHC class II biotin (N22), CD11c PE-Cy7 (N418; eBioscience), CD11b APC (M1-70; eBioscience), CD103 (2E7; eBioscience), Siglec-F APC (BD; lightning link APC conjugated [Novus Biologicals]) and CD40 PE (3/23; BD). FACS was performed on an LSRII or Fortessa (BD) and analyzed using FlowJo software (Tree Star) using standard protocols.

OVA sensitization and challenge protocol. We used the murine model of asthma based on OVA and adjuvant administration (Blyth et al., 1996). In brief, endotoxin-depleted OVA (Sigma-Aldrich; 0.25 mg/ml in alum [Sigma-Aldrich], 5 mg/ml; Aida and Pabst, 1990) in a total volume of 200 µl was injected i.p. on days 0, 7, and 14. Challenge with OVA (100 µg in 40 µl PBS) or PBS alone i.n. was performed on days 21, 22, and 23.

Lung and trachea dissection and dissociation. Mice were given a lethal dose of Avertin and exsanguinated from the descending aorta before lung dissection. Trachea, heart, lungs, and LN were removed from the chest cavity together. Lung lobes and trachea were separated and placed into dissociation medium composed of RPMI with 10% FCS, 400 U/ml collagenase D (Roche), and 0.25 mg/ml DNase I (Boehringer Ingelheim). Lobes and trachea were cut into small pieces with a razor blade and placed at 37°C for 30 min with pipetting to dissociate the tissue. Resulting cells were filtered through a 100-µm filter, separated from dead cells and debris with a Histopaque (Sigma-Aldrich) gradient, and stained for FACS or sorting.

Preparation of lung sections for live cell imaging in the lung. Lung sections were prepared for culture using methods similar to those used in studying lung smooth muscle contraction (Bergner and Sanderson, 2002, 2003; Delmotte and Sanderson, 2006), extending older methods of thick tissue sections (Dandurand et al., 1993). Mice were given a lethal overdose of Avertin and exsanguinated by cutting the descending aorta. The lungs and trachea were exposed by cutting through the diaphragm and chest wall. The mice were intubated by tracheotomy with the sheath from an 18-gauge i.v. catheter. Lungs were inflated with 1 ml of 2% low melting temp agarose (BMA) in sterile PBS maintained at 37°C, and the solution was solidified by briefly rinsing the inflated lungs with PBS at 4°C. Inflated lungs were then excised from the mouse and placed in a sterile 50-ml conical containing RT RPMI without phenol red (Invitrogen). The left lobe was isolated, cut into ∼300-µm sections using a vibratome filled with cool PBS, mounted on plastic slides with Vetbond (3M), and placed in a dish containing RT RPMI without phenol red before imaging.

LPS treatment of lung slices. Lung sections were prepared as listed in the previous section. A time lapse was collected before treatment. At t = 0, oxygenated media was replaced with oxygenated RPMI with 1 µg/ml LPS (Sigma-Aldrich). Media with LPS was continuously flowed over the section throughout the experiment. Time lapses were recorded starting at t = 10 min and t = 3 h.

Real-time two-photon imaging. A custom resonant-scanning two-photon instrument (Bullen et al., 2009) contains a four-photomultiplier tube detector and collects data at video rate. Where indicated, lung sections were stained with Hoechst for 20 min at a concentration of 100 ng/ml and then maintained at 36°C in RPMI medium bubbled with 95% O_2 and 5% CO_2 for up to 5 h. The health of lung sections was assessed by ciliary movement in large airways. Samples were excited with a 10-W Mai Tai Ti:Sapphire laser (Spectra-Physics) tuned to a wavelength of 910 nm, and emission wavelengths of 440/40 nm (for Hoechst and CFP), 505/20 nm (for GFP), 542/27 nm (for YFP), and 605/70 nm (for beads) were collected. A custom four-dimensional acquisition module in Video Savant digital video recording software (IO Industries) was used for image acquisition. Each lung section was first surveyed in a raster scan spanning 1567 µm × 1300 µm × 175 µm in xyz. For time-lapse acquisition, each xy stack spans 313 µm × 260 µm at a resolution of 0.653 µm per pixel spaced 1 µm apart for ∼100 µm in z, and 10–20 video-rate frames were averaged.

Live lung imaging. Mice were anesthetized with 80 mg/kg Ketamine and 12 mg/kg Xylazine i.p. and placed on a custom, heated microscope stage. Mice were mechanically ventilated with pressure control ventilation. Isoflurane was continuously delivered at 1% to maintain anesthesia, and mice were given an i.p. bolus of 1 ml PBS before the thoracic surgical procedure. The left lung was carefully exposed. The custom thoracic suction window attached to a micromanipulator on the microscope stage was then placed into position, and 20–25 mmHg of suction was applied (Amvex Corporation) to gently immobilize the lung. The two-photon microscope objective was then lowered into place over the thoracic suction window and a 12 mm coverslip.

Imaris-based analysis of motility and morphology. Images were analyzed with Imaris software (Bitplane) using isosurface with masking and spot tracker applications. Three-dimensional images were rendered by Imaris or MetaMorph software (Molecular Devices), and sphericity was calculated by Imaris using the

ratio of the surface area of a sphere (with the same volume as the given particle) to the surface area of the particle with the following equation:

$$\Psi = \frac{\pi^{1/3}(6V_p)^{2/3}}{A_p},$$

where V_p is the volume of the particle and A_p is the surface area of the particle.

T cell transfers. Naive CD2-RFP OTII cells were isolated and transferred immediately. A single cell suspension was isolated from LNs and spleens of CD2-RFP/OTII TCR transgenic mice. Naive CD4 T cells were purified using the EasySep CD4-negative selection kit (STEMCELL Technologies). T cells were transferred into CD11c-EYFP Actin-CFP mice via retroorbital injection.

Statistics. Data are presented as mean ± SEM. P-values were determined by performing a two-tailed Student's *t* test or an analysis of variance as necessary using Prism 5 (GraphPad Software).

Tissue fixation for static microscopy. Mice were overdosed with Avertin, the descending aorta was cut to drain excess blood from the chest cavity, and lungs were filled with 1 ml OCT (Tissue-Tek). The left lobe was tied off and frozen in OCT using liquid nitrogen and stored at −80°C until use. 7-mm sections were cut at −20°C using a cryostat and stained with fluorescent antibodies using a TSA amplification kit (Invitrogen). Tissues were examined with a spinning disk confocal microscope (Yokogawa Instruments) and analyzed using MetaMorph.

Online supplemental material. Fig. S1 describes the FACS gating strategy for DC subsets in the lung in PBS- and OVA-challenged mice. Fig. S2 describes the slice lung imaging method. Video 1 depicts real-time brightfield imaging of a large airway in a lung section 2 h after sectioning showing ciliary movement on the surface of a large airway. Video 2 depicts live imaging of a lung section showing DC motility in airway-adjacent and alveolar regions. Video 3 depicts migration of neutrophils and AMs in a control lung assessed using *c-fms*–EGFP marking. Video 4 depicts live imaging of a lung section showing DC motility in airway-adjacent regions. Video 5 depicts live imaging of a lung section showing sentinel DC motility in an airway-adjacent region. Video 6 depicts live imaging of a lung section showing a DC probing the airway epithelium. Video 7 depicts live imaging of a lung section showing dendrites sampling alveoli. Video 8 depicts live imaging of a lung section showing dendrites projecting beyond the alveolar epithelium. Video 9 depicts live imaging of alveoli in an intact lung showing dendrites sampling alveoli. Video 10 depicts live imaging of a lung section showing dendrites projecting beyond the alveolar epithelium to sample fluorescently labeled beads. Video 11 depicts live imaging of a lung section showing a DC present in the airway-adjacent region carrying an inhaled fluorescent bead. Video 12 depicts live imaging of a lung section showing antigen-specific T cells interacting with airway-adjacent DCs. Video 13 depicts live imaging of a lung section showing calcium flux of an antigen-specific T cell in contact with an airway-adjacent DC. Online supplemental material is available at http://www.jem.org/cgi/content/full/jem.20112667/DC1.

We thank Fred Siedenberg and Larry Braun (Sutter Instruments) and Sebastian Peck, Jessica Wong (University of California, San Francisco [UCSF] Biological Imaging Development Center), Caitlin Sorensen, and Omar Kahn for assistance with microscopy. We also thank Shuwei Jiang for FACS sorting, members of the UCSF Lung Biology Center for helpful discussion, and Alex Greer and Jun-Sook Shin for help with confocal staining.

This work was supported by the National Science Foundation graduate research fellowship program, the Strategic Asthma Basic Research, the American Asthma Foundation, and the National Institutes of Health (grant PO1 HL024136).

The authors have no competing financial interests.

Author contributions: E.E. Thornton designed and performed the experiments, collected and analyzed data, and wrote the manuscript. M.R. Looney, O. Bose, and D. Sen performed experiments and collected data. D. Sheppard and R. Locksley participated in the conception of experiments and edited the manuscript. X. Huang performed experiments. M.F. Krummel designed and performed experiments, provided administrative and financial support, and wrote the manuscript.

Submitted: 15 December 2011
Accepted: 19 April 2012

REFERENCES

Aida, Y., and M.J. Pabst. 1990. Removal of endotoxin from protein solutions by phase separation using Triton X-114. *J. Immunol. Methods.* 132:191–195. http://dx.doi.org/10.1016/0022-1759(90)90029-U

Ballesteros-Tato, A., B. León, F.E. Lund, and T.D. Randall. 2010. Temporal changes in dendritic cell subsets, cross-priming and costimulation via CD70 control CD8(+) T cell responses to influenza. *Nat. Immunol.* 11: 216–224. http://dx.doi.org/10.1038/ni.1838

Belz, G.T., C.M. Smith, L. Kleinert, P. Reading, A. Brooks, K. Shortman, F.R. Carbone, and W.R. Heath. 2004. Distinct migrating and non-migrating dendritic cell populations are involved in MHC class I-restricted antigen presentation after lung infection with virus. *Proc. Natl. Acad. Sci. USA.* 101:8670–8675. http://dx.doi.org/10.1073/pnas.0402644101

Bergner, A., and M.J. Sanderson. 2002. Acetylcholine-induced calcium signaling and contraction of airway smooth muscle cells in lung slices. *J. Gen. Physiol.* 119:187–198. http://dx.doi.org/10.1085/jgp.119.2.187

Bergner, A., and M.J. Sanderson. 2003. Airway contractility and smooth muscle Ca(2+) signaling in lung slices from different mouse strains. *J. Appl. Physiol.* 95:1325–1332, discussion :1314.

Blank, F., B. Rothen-Rutishauser, and P. Gehr. 2007. Dendritic cells and macrophages form a transepithelial network against foreign particulate antigens. *Am. J. Respir. Cell Mol. Biol.* 36:669–677. http://dx.doi.org/10.1165/rcmb.2006-0234OC

Blyth, D.I., M.S. Pedrick, T.J. Savage, E.M. Hessel, and D. Fattah. 1996. Lung inflammation and epithelial changes in a murine model of atopic asthma. *Am. J. Respir. Cell Mol. Biol.* 14:425–438.

Bullen, A., R.S. Friedman, and M.F. Krummel. 2009. Two-photon imaging of the immune system: a custom technology platform for high-speed, multicolor tissue imaging of immune responses. *Curr. Top. Microbiol. Immunol.* 334:1–29. http://dx.doi.org/10.1007/978-3-540-93864-4_1

Byersdorfer, C.A., and D.D. Chaplin. 2001. Visualization of early APC/T cell interactions in the mouse lung following intranasal challenge. *J. Immunol.* 167:6756–6764.

Cahalan, M.D., and I. Parker. 2008. Choreography of cell motility and interaction dynamics imaged by two-photon microscopy in lymphoid organs. *Annu. Rev. Immunol.* 26:585–626. http://dx.doi.org/10.1146/annurev.immunol.24.021605.090620

Chieppa, M., M. Rescigno, A.Y.C. Huang, and R.N. Germain. 2006. Dynamic imaging of dendritic cell extension into the small bowel lumen in response to epithelial cell TLR engagement. *J. Exp. Med.* 203:2841–2852. http://dx.doi.org/10.1084/jem.20061884

Dandurand, R.J., C.G. Wang, N.C. Phillips, and D.H. Eidelman. 1993. Responsiveness of individual airways to methacholine in adult rat lung explants. *J. Appl. Physiol.* 75:364–372.

Delmotte, P., and M.J. Sanderson. 2006. Ciliary beat frequency is maintained at a maximal rate in the small airways of mouse lung slices. *Am. J. Respir. Cell Mol. Biol.* 35:110–117. http://dx.doi.org/10.1165/rcmb.2005-0417OC

Desch, A.N., G.J. Randolph, K. Murphy, E.L. Gautier, R.M. Kedl, M.H. Lahoud, I. Caminschi, K. Shortman, P.M. Henson, and C.V. Jakubzick. 2011. $CD103^+$ pulmonary dendritic cells preferentially acquire and present apoptotic cell–associated antigen. *J. Exp. Med.* 208:1789–1797. http://dx.doi.org/10.1084/jem.20110538

Germain, R.N., M.J. Miller, M.L. Dustin, and M.C. Nussenzweig. 2006. Dynamic imaging of the immune system: progress, pitfalls and promise. *Nat. Rev. Immunol.* 6:497–507. http://dx.doi.org/10.1038/nri1884

Grayson, M.H., M.S. Ramos, M.M. Rohlfing, R. Kitchens, H.D. Wang, A. Gould, E. Agapov, and M.J. Holtzman. 2007. Controls for lung dendritic cell maturation and migration during respiratory viral infection. *J. Immunol.* 179:1438–1448.

Hadjantonakis, A.-K., S. Macmaster, and A. Nagy. 2002. Embryonic stem cells and mice expressing different GFP variants for multiple non-invasive reporter usage within a single animal. *BMC Biotechnol.* 2:11. http://dx.doi.org/10.1186/1472-6750-2-11

Hamilton-Easton, A., and M. Eichelberger. 1995. Virus-specific antigen presentation by different subsets of cells from lung and mediastinal lymph node tissues of influenza virus-infected mice. *J. Virol.* 69:6359–6366.

Hammad, H., and B.N. Lambrecht. 2007. Lung dendritic cell migration. *Adv. Immunol.* 93:265–278. http://dx.doi.org/10.1016/S0065-2776(06)93007-7

Hammad, H., and B.N. Lambrecht. 2008. Dendritic cells and epithelial cells: linking innate and adaptive immunity in asthma. *Nat. Rev. Immunol.* 8:193–204. http://dx.doi.org/10.1038/nri2275

Hammad, H., M. Chieppa, F. Perros, M.A. Willart, R.N. Germain, and B.N. Lambrecht. 2009. House dust mite allergen induces asthma via Toll-like receptor 4 triggering of airway structural cells. *Nat. Med.* 15:410–416. http://dx.doi.org/10.1038/nm.1946

Hammad, H., M. Plantinga, K. Deswarte, P. Pouliot, M.A.M. Willart, M. Kool, F. Muskens, and B.N. Lambrecht. 2010. Inflammatory dendritic cells—not basophils—are necessary and sufficient for induction of Th2 immunity to inhaled house dust mite allergen. *J. Exp. Med.* 207:2097–2111. http://dx.doi.org/10.1084/jem.20101563

Holt, P.G. 2005. Pulmonary dendritic cells in local immunity to inert and pathogenic antigens in the respiratory tract. *Proc. Am. Thorac. Soc.* 2:116–120. http://dx.doi.org/10.1513/pats.200502-017AW

Jahnsen, F.L., D.H. Strickland, J.A. Thomas, I.T. Tobagus, S. Napoli, G.R. Zosky, D.J. Turner, P.D. Sly, P.A. Stumbles, and P.G. Holt. 2006. Accelerated antigen sampling and transport by airway mucosal dendritic cells following inhalation of a bacterial stimulus. *J. Immunol.* 177:5861–5867.

Jakubzick, C., F. Tacke, J. Llodra, N. van Rooijen, and G.J. Randolph. 2006. Modulation of dendritic cell trafficking to and from the airways. *J. Immunol.* 176:3578–3584.

Jakubzick, C., M. Bogunovic, A.J. Bonito, E.L. Kuan, M. Merad, and G.J. Randolph. 2008a. Lymph-migrating, tissue-derived dendritic cells are minor constituents within steady-state lymph nodes. *J. Exp. Med.* 205:2839–2850. http://dx.doi.org/10.1084/jem.20081430

Jakubzick, C., J. Helft, T.J. Kaplan, and G.J. Randolph. 2008b. Optimization of methods to study pulmonary dendritic cell migration reveals distinct capacities of DC subsets to acquire soluble versus particulate antigen. *J. Immunol. Methods.* 337:121–131. http://dx.doi.org/10.1016/j.jim.2008.07.005

Kraft, M., G.H. Cassell, J.E. Henson, H. Watson, J. Williamson, B.P. Marmion, C.A. Gaydos, and R.J. Martin. 1998. Detection of Mycoplasma pneumoniae in the airways of adults with chronic asthma. *Am. J. Respir. Crit. Care Med.* 158:998–1001.

Kreisel, D., R.G. Nava, W. Li, B.H. Zinselmeyer, B. Wang, J. Lai, R. Pless, A.E. Gelman, A.S. Krupnick, and M.J. Miller. 2010. In vivo two-photon imaging reveals monocyte-dependent neutrophil extravasation during pulmonary inflammation. *Proc. Natl. Acad. Sci. USA.* 107:18073–18078. http://dx.doi.org/10.1073/pnas.1008737107

Lambrecht, B.N., and H. Hammad. 2009. Biology of lung dendritic cells at the origin of asthma. *Immunity.* 31:412–424. http://dx.doi.org/10.1016/j.immuni.2009.08.008

Lambrecht, B.N., B. Salomon, D. Klatzmann, and R.A. Pauwels. 1998. Dendritic cells are required for the development of chronic eosinophilic airway inflammation in response to inhaled antigen in sensitized mice. *J. Immunol.* 160:4090–4097.

Lindquist, R.L., G. Shakhar, D. Dudziak, H. Wardemann, T. Eisenreich, M.L. Dustin, and M.C. Nussenzweig. 2004. Visualizing dendritic cell networks in vivo. *Nat. Immunol.* 5:1243–1250. http://dx.doi.org/10.1038/ni1139

Looney, M.R., E.E. Thornton, D. Sen, W.J. Lamm, R.W. Glenny, and M.F. Krummel. 2011. Stabilized imaging of immune surveillance in the mouse lung. *Nat. Methods.* 8:91–96. http://dx.doi.org/10.1038/nmeth.1543

Lukens, M.V., D. Kruijsen, F.E.J. Coenjaerts, J.L.L. Kimpen, and G.M. van Bleek. 2009. Respiratory syncytial virus-induced activation and migration of respiratory dendritic cells and subsequent antigen presentation in the lung-draining lymph node. *J. Virol.* 83:7235–7243. http://dx.doi.org/10.1128/JVI.00452-09

Martin, R.J., M. Kraft, H.W. Chu, E.A. Berns, and G.H. Cassell. 2001. A link between chronic asthma and chronic infection. *J. Allergy Clin. Immunol.* 107:595–601. http://dx.doi.org/10.1067/mai.2001.113563

Martin, T.R., and C.W. Frevert. 2005. Innate immunity in the lungs. *Proc. Am. Thorac. Soc.* 2:403–411. http://dx.doi.org/10.1513/pats.200508-090JS

McWilliam, A.S., S. Napoli, A.M. Marsh, F.L. Pemper, D.J. Nelson, C.L. Pimm, P.A. Stumbles, T.N. Wells, and P.G. Holt. 1996. Dendritic cells are recruited into the airway epithelium during the inflammatory response to a broad spectrum of stimuli. *J. Exp. Med.* 184:2429–2432. http://dx.doi.org/10.1084/jem.184.6.2429

Miller, M.J., S.H. Wei, I. Parker, and M.D. Cahalan. 2002. Two-photon imaging of lymphocyte motility and antigen response in intact lymph node. *Science.* 296:1869–1873. http://dx.doi.org/10.1126/science.1070051

Miller, M.J., S.H. Wei, M.D. Cahalan, and I. Parker. 2003. Autonomous T cell trafficking examined in vivo with intravital two-photon microscopy. *Proc. Natl. Acad. Sci. USA.* 100:2604–2609. http://dx.doi.org/10.1073/pnas.2628040100

Pedroza-González, A., G.S. García-Romo, D. Aguilar-León, J. Calderon-Amador, R. Hurtado-Ortiz, H. Orozco-Estevez, B.N. Lambrecht, I. Estrada-García, R. Hernández-Pando, and L. Flores-Romo. 2004. In situ analysis of lung antigen-presenting cells during murine pulmonary infection with virulent *Mycobacterium tuberculosis*. *Int. J. Exp. Pathol.* 85:135–145. http://dx.doi.org/10.1111/j.0959-9673.2004.00381.x

Rescigno, M., M. Urbano, B. Valzasina, M. Francolini, G. Rotta, R. Bonasio, F. Granucci, J.P. Kraehenbuhl, and P. Ricciardi-Castagnoli. 2001. Dendritic cells express tight junction proteins and penetrate gut epithelial monolayers to sample bacteria. *Nat. Immunol.* 2:361–367. http://dx.doi.org/10.1038/86373

Robinson, D.S., Q. Hamid, S. Ying, A. Tsicopoulos, J. Barkans, A.M. Bentley, C. Corrigan, S.R. Durham, and A.B. Kay. 1992. Predominant TH2-like bronchoalveolar T-lymphocyte population in atopic asthma. *N. Engl. J. Med.* 326:298–304. http://dx.doi.org/10.1056/NEJM199201303260504

Sasmono, R.T., D. Oceandy, J.W. Pollard, W. Tong, P. Pavli, B.J. Wainwright, M.C. Ostrowski, S.R. Himes, and D.A. Hume. 2003. A macrophage colony-stimulating factor receptor-green fluorescent protein transgene is expressed throughout the mononuclear phagocyte system of the mouse. *Blood.* 101:1155–1163. http://dx.doi.org/10.1182/blood-2002-02-0569

Sung, S.-S.J., S.M. Fu, C.E. Rose Jr., F. Gaskin, S.-T. Ju, and S.R. Beaty. 2006. A major lung CD103 (alphaE)-beta7 integrin-positive epithelial dendritic cell population expressing Langerin and tight junction proteins. *J. Immunol.* 176:2161–2172.

Takano, K.-I., T. Kojima, M. Go, M. Murata, S. Ichimiya, T. Himi, and N. Sawada. 2005. HLA-DR- and CD11c-positive dendritic cells penetrate beyond well-developed epithelial tight junctions in human nasal mucosa of allergic rhinitis. *J. Histochem. Cytochem.* 53:611–619. http://dx.doi.org/10.1369/jhc.4A6539.2005

Tan, W.C. 2005. Viruses in asthma exacerbations. *Curr. Opin. Pulm. Med.* 11:21–26.

van Rijt, L.S., J.B. Prins, P.J. Leenen, K. Thielemans, V.C. de Vries, H.C. Hoogsteden, and B.N. Lambrecht. 2002. Allergen-induced accumulation of airway dendritic cells is supported by an increase in CD31(hi)Ly-6C(neg) bone marrow precursors in a mouse model of asthma. *Blood.* 100:3663–3671. http://dx.doi.org/10.1182/blood-2002-03-0673

van Rijt, L.S., S. Jung, A. Kleinjan, N. Vos, M. Willart, C. Duez, H.C. Hoogsteden, and B.N. Lambrecht. 2005. In vivo depletion of lung $CD11c^+$ dendritic cells during allergen challenge abrogates the characteristic features of asthma. *J. Exp. Med.* 201:981–991. http://dx.doi.org/10.1084/jem.20042311

Veiga-Fernandes, H., M.C. Coles, K.E. Foster, A. Patel, A. Williams, D. Natarajan, A. Barlow, V. Pachnis, and D. Kioussis. 2007. Tyrosine kinase receptor RET is a key regulator of Peyer's patch organogenesis. *Nature.* 446:547–551. http://dx.doi.org/10.1038/nature05597

Vermaelen, K.Y., I. Carro-Muino, B.N. Lambrecht, and R.A. Pauwels. 2001. Specific migratory dendritic cells rapidly transport antigen from the airways to the thoracic lymph nodes. *J. Exp. Med.* 193:51–60. http://dx.doi.org/10.1084/jem.193.1.51

Voehringer, D., T.A. Reese, X. Huang, K. Shinkai, and R.M. Locksley. 2006. Type 2 immunity is controlled by IL-4/IL-13 expression in hematopoietic non-eosinophil cells of the innate immune system. *J. Exp. Med.* 203:1435–1446. http://dx.doi.org/10.1084/jem.20052448

von Garnier, C., L. Filgueira, M. Wikstrom, M. Smith, J.A. Thomas, D.H. Strickland, P.G. Holt, and P.A. Stumbles. 2005. Anatomical location determines the distribution and function of dendritic cells and other APCs in the respiratory tract. *J. Immunol.* 175:1609–1618.

Wenzel, S., D. Wilbraham, R. Fuller, E.B. Getz, and M. Longphre. 2007. Effect of an interleukin-4 variant on late phase asthmatic response to allergen challenge in asthmatic patients: results of two phase 2a studies. *Lancet.* 370:1422–1431. http://dx.doi.org/10.1016/S0140-6736(07)61600-6

Wikstrom, M.E., and P.A. Stumbles. 2007. Mouse respiratory tract dendritic cell subsets and the immunological fate of inhaled antigens. *Immunol. Cell Biol.* 85:182–188.